Article

In Silico Screening of Chlorogenic Acids from Plant Sources against Human Translocase-I to Identify Competitive Inhibitors to Treat Diabetes

Pravin Kumar Ramalingam,* Manikandan Chandrasekaran, Poonam Gupta, Vinod Nelamangala Umesh, Tharun Bharadwaj, Naveen Banchallihundi Krishna, Roopa Lalitha, and Gladstone Sigamani Gunaseelan

Read Online

ACCESS | Metrics & More | Article Recommendations | Supporting Information

ABSTRACT: Chlorogenic acids (CHLs) are known to competitively bind to translocase-I (T1) of the glucose-6-phosphatase (G6 Pase) system, thereby inhibiting the transport of glucose-6-phosphate (G6P). This competitive binding results in a consequential reduction in blood sugar levels. In this study, steered molecular dynamics (SMD) simulation is employed to investigate the interaction between T1 and G6P, aiming to gain insights into the binding dynamics and diffusion process of G6P through T1. A database comprising 41 CHLs sourced from various plants was developed, subjected to minimization, and screened against T1 through conventional docking methods. The docked conformations were fed into a newly developed customized scoring method incorporating contact-based weights to assess the binding affinities that systematically rank and identify the most effective competitive inhibitors. Among the screened CHLs, 1-methoxy 3,5-dicaffeoylquinic acid, 3,4 dicaffeoyl quinic acid, and 3,4,5-tricaffeoylquinic acid stood out as the top three inhibitors, showcasing crucial atomic interactions with key residues within the binding pocket of T1, and these CHLs are sourced from readily available plants, diminishing reliance on coffee as the predominant CHL source. Along with the devised scoring function, which serves as a valuable tool for virtual screening and lead optimization in drug development, this study also marks a pioneering effort as it involves the modeling of the human translocase and unravels the mechanism of binding and diffusion of G6P within human T1, providing valuable insights into the structural prerequisites for successfully inhibiting the G6P system, laying the foundation for a rational approach to drug design. This research contributes to the progress of drug discovery strategies focused on the G6P system, presenting potential therapeutic avenues for addressing metabolic disorders linked to an impaired glucose metabolism.
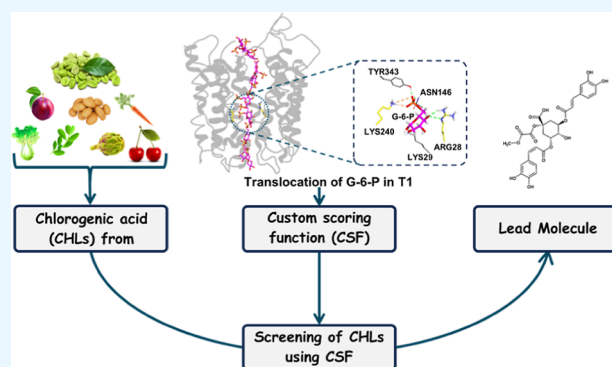
1. INTRODUCTION

The regulation of blood glucose levels is a critical aspect of maintaining overall health and preventing metabolic disorders, such as diabetes. Numerous studies have investigated the impact of coffee consumption on blood glucose levels, revealing intriguing differences between caffeinated and decaffeinated coffee. Specifically, individuals who consume decaffeinated coffee exhibit lower blood glucose levels than those who consume an equivalent amount of caffeinated coffee.[1,2] These observations suggest the involvement of noncaffeine compounds in coffee that may influence the glucose metabolism and insulin sensitivity.[3] Among the noncaffeine compounds present in coffee, chlorogenic acids (CHLs) have gained considerable attention. One prominent example is 5-caffeoylquinic acid, a major chlorogenic acid abundantly found in coffee. Research has shown that CHLs possess properties that enhance glucose tolerance and insulin sensitivity, leading to improved glycemic control.[4,5] Mechanistically, CHLs are known to competitively inhibit the glucose-6-

phosphate (G6P) system, specifically targeting the glucose-6-phosphatase (G6 Pase) (T1) enzyme responsible for glucose metabolism.[6]

Despite the growing interest in CHLs as potential inhibitors of the G6P system, several key knowledge gaps remain unaddressed. First, the structural characterization of the T1 protein, as well as the mechanism of G6P diffusion through the enzyme, has not been thoroughly studied. Understanding the three-dimensional structure and active site of T1 is crucial for gaining molecular insights into its interactions with G6P and
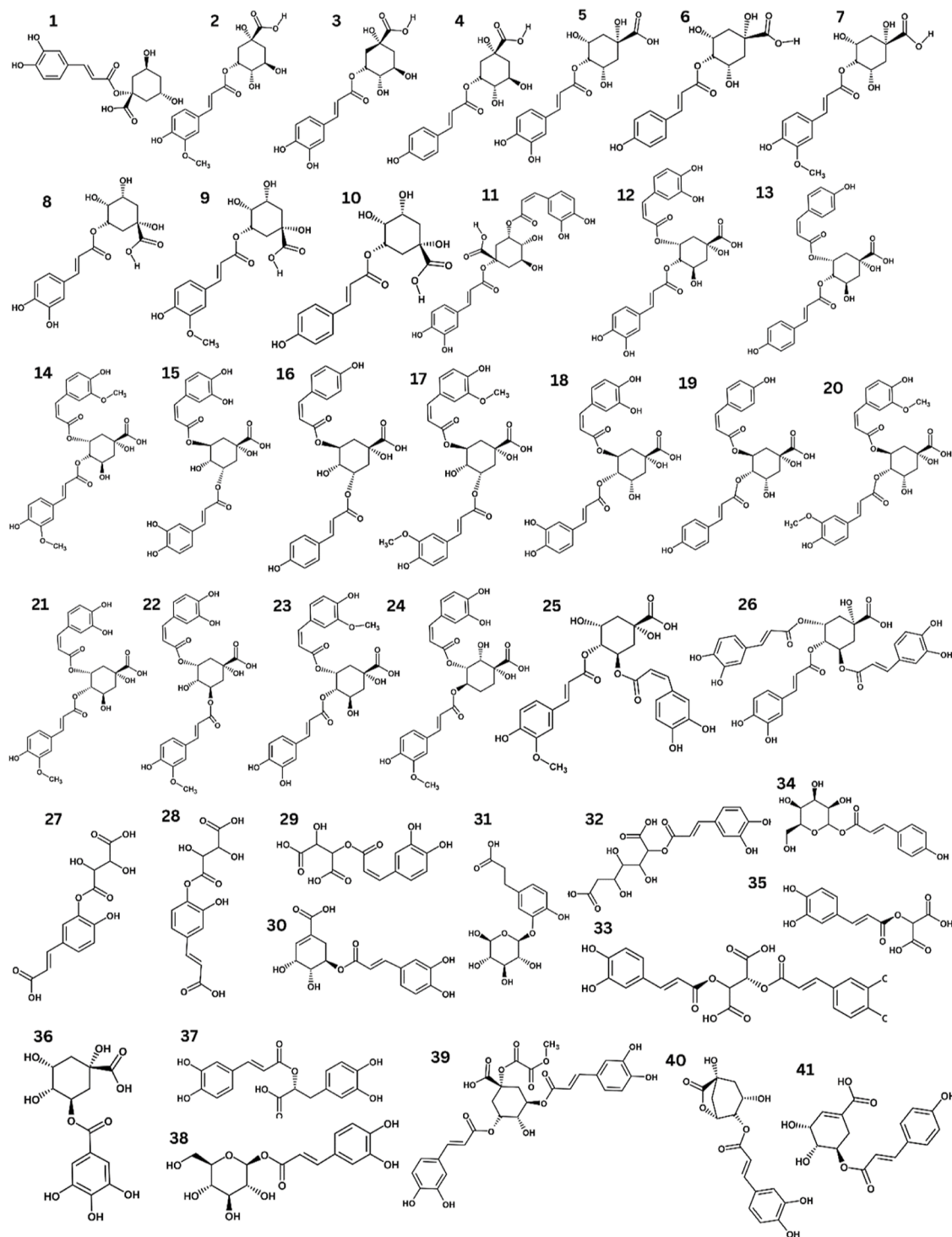
Figure 1. 2D Structures of 41 different CHLs from different plant sources such as green coffee beans, kale, cabbage, brussel sprouts, artichoke, etc. that were used in this study are listed.

for elucidating the precise mechanisms underlying its inhibitory effects.[7,8]

Moreover, although the inhibitory role of CHLs on the G6P system has been established, the exact binding site of CHLs and the crucial residue interactions required for drug design have not been reported. The absence of structural and binding mode studies for any of the CHLs hinders the rational design of potent inhibitors. Identifying the specific binding mode of CHLs and characterizing their interactions with T1 would

provide valuable templates for drug design efforts targeting the G6P system.

Therefore, this study aims to bridge these critical gaps in our understanding. We seek to unravel the structure of the T1 protein and investigate the mechanism of diffusion of G6P through the enzyme. Additionally, we aim to elucidate the binding site and crucial residue interactions of CHLs, which are essential for the rational design of effective inhibitors. By addressing these knowledge gaps, we hope to provide valuable

insights and templates for the development of novel drugs targeting the G6P system.

Through this research, we aim to shed light on the structural characterization of T1, elucidate the molecular interactions between T1 and G6P, and determine the binding mode of CHLs. These findings hold significant promise for the rational design of potent inhibitors,[8] paving the way for advancements in the treatment of conditions such as type 1 diabetes, brain tumor progression, and glycogen storage disease.[9−11]

2. RESULTS

2.1. Characterization of CHLs and Modeling of Human G6P T1. *2.1.1. Characterization of CHLs from Various Plant Sources Reveals Potential Inhibitors.* We compiled a comprehensive database comprising 41 CHLs sourced from a variety of plants, including green coffee beans, kale, cabbage, Brussels sprouts, and artichoke. These CHLs exhibit diverse 2D structures, as depicted in Figure 1. Table S1 provides detailed information on the names and plant sources of each CHL. Through this extensive collection, we aimed to identify novel CHLs that could serve as competitive inhibitors of G6P and target the G6Psystem.

2.1.2. Modeling of the Human G6P T1 Protein Structure Sheds Light on the G6P Diffusion Mechanism. Using SWISS-Model with 1pw4.1.A as a template (100% sequence identity), we successfully predicted the structure of human G6P T1. The resulting modeled structure demonstrated a high percentage (91.18%) of residues falling within the favored regions of the Ramachandran plot, indicating its reliability. To determine the positioning of the modeled G6P T1 within the membrane, we employed the PPM web server, as shown in Figure 2. Table S2
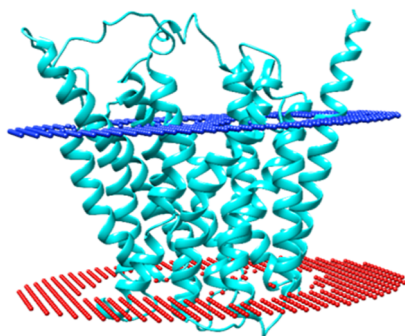
Figure 2. Cyan ribbon represents the modeled human G6P translocase SLC37A4 isoform 1 using 1PW4.1 as the template and red and blue dotted planes depict the predicted membrane surface.

provides additional information about available templates used for modeling G6P T1. The accurate modeling of the T1 protein structure sets the stage for understanding its functional mechanism and interaction with potential inhibitors.

2.1.3. Docking and Molecular Dynamics Simulations Unveil the Binding Mode of G6P in T1. By subjecting the optimized modeled structure of G6P T1 to docking with G6P, we obtained a binding energy of −6.550 kcal/mol, suggesting a stable interaction. Subsequently, we performed molecular dynamics (MD) simulations to gain insights into the binding mode and dynamics of the T1−G6P complex. The MD simulations, conducted for a duration of 5 ns and repeated four times, revealed the most favorable binding mode of G6P within the T1 protein, as depicted in Figure 3. It is noteworthy that G6P occupied a specific pocket formed by critical residues,
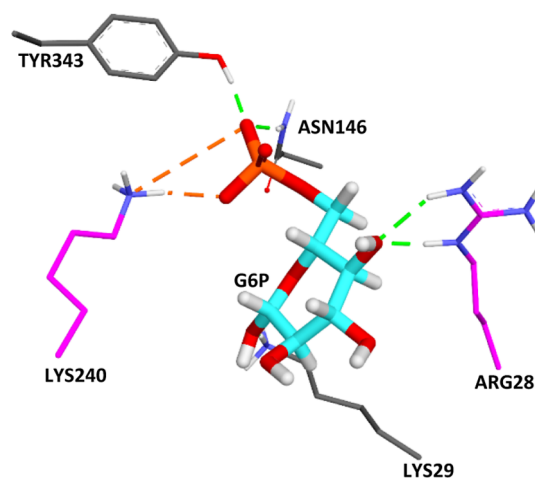
Figure 3. Interactions of G6P with translocase-I as obtained from MD simulation. The G6P has a salt bridge with LYS240 and ARG28 (magenta sticks), which are the active site residues; other residues like ASN146, TYR343, and LYS29 found anchoring G6P to stabilize the conformation in the pocket.

including Arg28, Lys29, Asn146, Lys240, and Tyr343. Notably, hydrogen bond interactions were observed between G6P and Arg28, Lys29, Asn146, and Tyr343. Furthermore, salt bridge and charge−charge interactions were identified with Lys240. These findings provide valuable insights into the crucial residues involved in the binding of G6P and pave the way for a rational drug design.

2.1.4. Insights from Steered Molecular Dynamics Simulation Illuminate the G6P Diffusion Mechanism. To further investigate the dynamic behavior of G6P within T1, we conducted steered molecular dynamics (SMD) simulations. The SMD simulations allowed us to observe the interactions and contact amino acids of G6P along the pore of T1. Notably, we observed maximum contacts between G6P and the enzyme when G6P reached the narrow region of the funnel, represented by the bottleneck between Lys240 and Arg28. Frames 7 to 30 across the SMD simulations demonstrated the stepwise diffusion of G6P from the wider region of T1 toward the narrow bottleneck region. Noteworthy interactions between G6P and residues Thr53, Ser32, and Asp245 were also observed, contributing to the stabilization of the G6P conformation within the binding pocket. These findings shed light on the intricate process of G6P diffusion and highlight the critical amino acids involved in the process (Figure 4).

2.1.5. Virtual Screening and Molecular Descriptor Calculations Identify Potential CHL Inhibitors. To identify potential inhibitors, we subjected 41 CHLs from our database to virtual screening against the modeled T1 protein. The binding energies and molecular descriptors, including ADMET properties, were calculated by using MOLE db. Table S3 presents the comprehensive results of the virtual screening, revealing that the CHLs exhibited improved binding energies compared to those of G6P (−6.55 kcal/mol). This suggests that certain CHLs have the potential to serve as effective inhibitors of T1 and opens up possibilities for the design of novel drugs targeting the G6P system.

2.1.6. Customized Scoring Function to Screen CHLs. A new scoring function to rank the docked conformations of chlorogenic acid was developed, the derivation of which is explained below. G6P was docked against the modeled T1, and
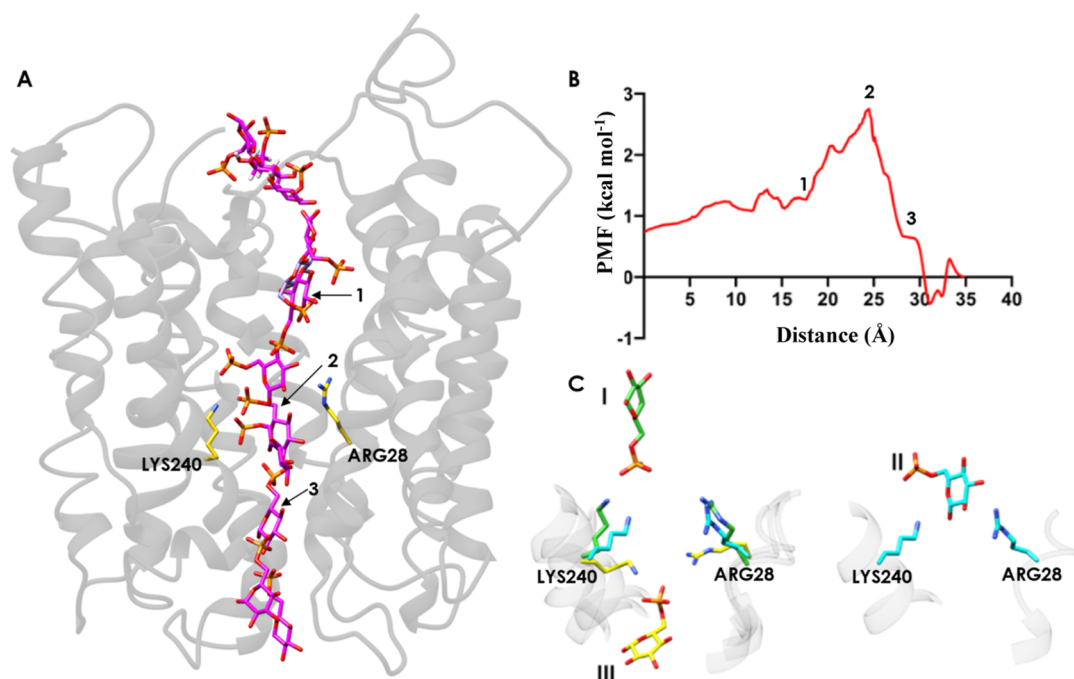
Figure 4. (A) Translocation of G6P where the substrate is shown in light pink sticks and active site residues are shown in yellow sticks. (B) Potential mean force taken by the substrate during the translocation process. (C) The substrate must change its conformation in order to move through the active site. In the event of translocation, 1, 2, and 3 in (A) are reference conformations corresponding to positions 1, 2, and 3 in (B), respectively, where the energy and dynamical movement of the substrate are observed more. The G6P found translocating from one end of the membrane to another is the membrane defined in Figure 2. The SMD simulation helped identify the residues interacting with G6P during the translocation process and the role of charged residues in the pocket. The umbrella sampling studies revealed the energetical movement and conformational transition of G6P and catalytic residues Arg28 and Lys240. As G6P moves toward the pocket, the energy increases (B 1, 2) because of the conformational changes. As it moves outside the pocket where Arg28 and Lys240 anchor and releases G6P, indicating the utilization of less energy (B 3). The Arg28 and Lys240 play a crucial role in the translocation of G6P, as it undergoes a conformational change to facilitate the diffusion of G6P. These two residues hold and anchor the movement of the substrate as it moves through the protein (C I–III).

these conformations were subjected to a python script that calculated contacts between the atoms of G6P and T1 using the van der Waals (VDW) radii. For detecting contacts, negative cutoff values of 0.0 to −1.0 Å with an allowance of 0.0 Å alongside the overlap between the interacting atoms were calculated using the equation

$$\text{overlap}_{ij} = r_{\text{VDWi}} + r_{\text{VDWj}} - d_{ij} - \text{allowance}_{ij} \tag{1}$$

The distance calculated for each contact derived from the above equation was inversed ($1/c$), where c is the contact distance, so that it can be summed up to give a cumulative weight for each interacting amino acid. This is based on the axiom that the greater the distance, the smaller the interactive capacity and vice versa. For each amino acid that interacts with the G6P, the contact score was summated for a specific atom type of the amino acid. For example, the CZ of Arg28 interacts with the phosphate oxygen of G6P and it formed 6 contacts, and CZ had a sum of 4.909 as the weight.

2.1.7. Derivation of the Customized Scoring Function.
2.1.7.1. Weight of all the Atoms of the Reference Ligand and Heavy Atoms of Residues.

$$\alpha_{\text{AB}} = \sum_{i=0}^{n} \frac{1}{(D_{\text{AB}})_i} \tag{2}$$

where A = (generalized) all the atoms of the reference ligand. $n \in \{O, C, H, A, S, N\}$, B = all the (Autodock based) heavy atom types of each residue, n = number of conformations of the reference ligand having the specific (A, B) combination,

and $D_{\text{AB}} = \sqrt{(x_A - x_B)^2 + (y_A - y_B)^2 + (z_A - z_B)^2}$ = Euclidean distance from A to B, where, x, y, z = Cartesian coordinates of the reference ligand (A) (in the ith conformation) or amino acid (B).

2.1.7.2. Weight of all the Atoms of the Drugs and Heavy Atoms of Residues.

$$\beta_{\text{AB}} = \sum_{i=0}^{n} \frac{1}{(D_{\text{AB}})_i} \tag{3}$$

where A = (generalized) all the atoms of drugs. $n \in \{O, C, H, A, S, N, P\}$, B = all the (Autodock based) heavy atom types of each residue, and n = number of conformations of drug having the (A, B) combinations.

2.1.7.3. Score Generated for Each Pair of Atoms of Drug and Heavy Atom Type of Residues.

$$S_{\text{AB}} = \alpha_{\text{AB}} \beta_{\text{AB}} \tag{4}$$

where A = (generalized) all the atoms of drugs. $n \in \{O, C, H, A, S, N, P\}$, B = all the heavy (Autodock based) atom types of each residue, α_{AB} = score of A–B (ligand–protein) atom combination (from eq 2), and β_{AB} = score of A–B (ligand–protein) atom combination with respect to the reference ligand (from eq 3).

2.1.7.4. Final Score for a Drug.

$$\text{Score} = \sum S_N \tag{5}$$
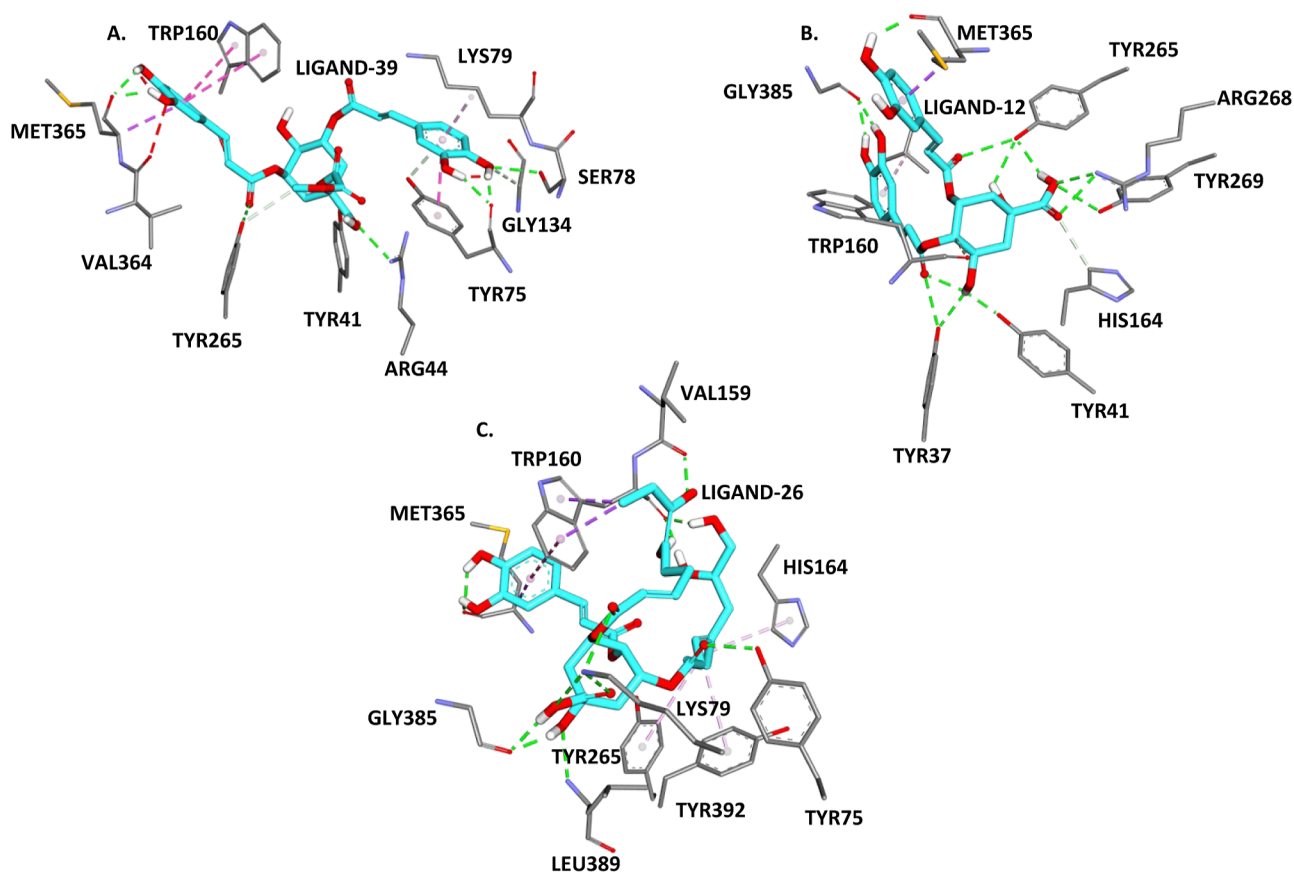
Figure 5. Interactions of top 3 compounds based on docking scores derived from the customized scoring function. (A) shows interactions of 1-methoxy 3,5-dicaffeoylquinic with T1. (B) shows interactions of 3,4 dicaffeoyl quinic acid with T1. (C) shows interactions of 3,4,5-tricaffeoylquinic acid with T1. In all cases, H-bonds are shown in green dotted lines, pi−cation interactions are shown in orange dotted lines, pi−alkyl interactions are shown in light pink dotted lines, pi−sigma interactions are shown in purple dotted lines, and amide−pi stack interactions are shown in pink dotted lines.

where N = set of all A−B (drug−protein) atom combinations existing for a single drug and S_N = calculated score for the "N" protein−drug pair for a single drug.

2.1.8. Contact-Based Screening and Binding Free Energy Calculation Using the Customized Scoring Function Reveals Promising CHL Candidates. To evaluate the potential binding of CHLs to the T1 protein, we employed a contact-based screening approach using a weight matrix and a customized scoring function. We calculated weights for each atom of the amino acids in contact with the atoms of G6P by using the established protocol. Next, we mapped the atoms of each CHL to the atom types of the T1 amino acids, specifically oxygen (O), aliphatic carbon (CC), aromatic carbon (AC), and hydrogen (H). The docking scores for the 41 CHLs were then calculated using the aforementioned protocol, and the results are presented in Table S4.

2.1.9. Compounds with High Docking Scores and Binding Modes. Among the tested compounds, three CHLs demonstrated particularly high docking scores (derived using the customized scoring function): 1-methoxy 3,5-dicaffeoylquinic acid, 3,4-dicaffeoyl quinic acid, and 3,4,5-tricaffeoylquinic acid. Their respective docking scores were 1402.039, 1346.889, and 1308.759. Figure 5 illustrates the binding modes of these three top compounds within the T1 protein.

1-Methoxy 3,5-dicaffeoylquinic acid was observed to form hydrogen bond interactions with residues Tyr 25, Gln 56, Tyr 343, and Ile 346. Additional interacting residues included Lys

64, Leu 141, His 366, and Leu 371, which formed pi-alkyl contacts. Furthermore, a pi−cation interaction was observed with Arg 28 and Lys 64.

For 3,4-dicaffeoyl quinic acid, hydrogen bond interactions were observed with residues Lys 64, Lys 240, and Tyr 343. Residues Leu 141, Met 145, and Ala 347 exhibited pi−alkyl interactions with the ligand. Other interactions included pi−sigma bonds and an amide−pi stack with Ile 346. In the case of 3,4,5-tricaffeoylquinic acid, hydrogen bond interactions were observed with residues Leu 141, Ser 142, Lys 240, Ala 347, Ala 367, and Gly 370. A pi−donor interaction was identified with Tyr 343. Additionally, pi−sigma interactions with Met 154 and Leu 141, as well as pi−alkyl interactions with Ala 347, were observed.

These findings highlight the specific amino acid residues involved in the interactions between the tested CHLs and the T1 protein. The diverse binding modes and favorable interactions suggest that these CHLs hold promise as potential inhibitors for further drug design efforts.

3. DISCUSSION

This study establishes a robust foundation for advancing drug design and development targeting the G6 Pase system. The identification of CHLs as potential inhibitors of G6P, coupled with their favorable binding characteristics, opens avenues for the design of novel therapeutic agents. Building upon the

insights gained from this study, several implications for further drug design can be considered.

The application of SMD, a technique that examines the behavior of small molecules through the application of an external bias force, has been proven instrumental. This method enabled the investigation of G6P diffusion through T1, exploring the key residues responsible for its interaction and facilitating its diffusion. Multiple binding modes of G6P during translocation through T1, coupled with their respective potential mean forces, were analyzed. This analysis unveiled the pivotal role of positively charged residues, specifically LYS240 and ARG28 located at the center of the diffusion path, in guiding G6P through the tunnel. This newfound insight played a crucial role in defining a potential drug-binding target for screening CHLs, a detail not previously disclosed in any prior studies.

The detailed characterization of the binding modes and key interacting residues between the CHLs and the T1 protein provides a structural basis for a rational drug design. The specific hydrogen bond interactions, pi—alkyl contacts and pi—pi, pi—cation, and pi—sigma bonds identified in the CHL—T1 complexes highlight critical residues that contribute to the binding affinity. This knowledge can guide the design of small molecules or derivatives with enhanced interactions and improved inhibitory potency. Structural modifications of the CHL scaffold, such as substitutions or additions, can be explored to optimize the binding affinity and selectivity.

Furthermore, the developed customized scoring function can serve as a valuable tool for the evaluation of new compounds or analogues in virtual screening and lead optimization processes. By considering the specific atom—atom contacts and incorporating weights derived from contact-based analysis, this scoring function provides a tailored approach for predicting binding energies. This can assist in prioritizing potential drug candidates for further experimental validation and optimization, streamlining the drug discovery process.

In addition to the CHLs identified in this study, the database can be expanded to include a broader range of compounds, natural or synthetic, with similar structural features. Virtual screening of such compounds against the T1 protein, using the established scoring function, may lead to the identification of novel lead molecules with improved pharmacological properties. This approach broadens the scope for drug design beyond the CHLs studied here and increases the chances of discovering more potent and selective inhibitors. CHLs contain a quinic acid moiety, derived from tetrahydroxycyclohexane carboxylic acid, which serves as a negatively charged functional group. This moiety actively interacts with positively charged residues situated along the substrate diffusion path of T1. Notably, the quinic acid moiety within CHLs showcases inherent pharmacophoric features, emphasizing its significance in fostering interactions within the T1 substrate diffusion path.

Moreover, this study highlights the importance of considering diverse plant sources as potential reservoirs of bioactive compounds. By exploring CHLs from various botanical origins, researchers can tap into the rich chemical diversity present in nature. This expands the pool of compounds available for drug design and reduces the reliance on a single source, such as coffee. Future studies can focus on screening CHLs from different plant species, including those with traditional medicinal uses or those known for their bioactive phytochemical profiles. This approach may lead to the discovery of new CHLs with improved properties or novel scaffolds for G6P inhibition.

4. CONCLUSIONS

The modeling of T1 and the subsequent SMD study conducted to investigate the diffusion of G6P through T1 aided in defining the potential drug-binding target for screening CHLs, a detail not previously disclosed in any prior studies. The elucidation of the binding modes and the development of a tailored scoring function to explore a spectrum of CHLs from diverse plant origins collectively contribute to expanding the knowledge base. Through the meticulous assessment and ranking of 41 CHLs sourced from various plants, this research provides valuable insights into the potential of CHLs as inhibitors of the G6P system, and this study also sets the stage for further drug design endeavors. This expanded understanding serves as a catalyst for designing and optimizing novel CHL-based inhibitors, with the potential to revolutionize treatments for conditions associated with the dysregulated glucose metabolism. The implications offer a beacon of hope in addressing complex metabolic disorders and fostering the development of innovative and more effective therapeutic interventions.

5. METHODS

5.1. Database Construction of CHLs from Various Sources. CHLs are generally esters formed between *trans*-cinnamic acid and quinic acid, which can be classified into mono, di, and mixed esters. Those which have only one *trans*-cinnamic acid attached to the quinic acid core make up mono esters. Diesters and triesters are made up by the attachment of one or two more *trans*-cinnamic acid(s) to the one already present in the monoesters, respectively. Mixed esters are those where two different *trans*-cinnamic acids are attached to the quinic acid.[12−17] CHLs of all these classes from different sources such as coffee, fruits, nuts, and vegetables wer characterized[18−22] and are brought together to make a one-stop database of 41CHLs. The 2D structures of the same are shown in Figure 1 in the Results section. The names and the sources of the same are provided in Table S1.

5.2. Docking of G6P and Virtual Screening of CHLs with Modeled T1. The Human Microsomal G6P Transporter (NP_001458 − G6P exchanger SLC37A4 isoform 1 − *Homo sapiens*) was modeled by Swissmodel[23] using 1PW4 as the template. The model obtained (Figure 2 shown in Results section) was subject to 1000 cycles of minimization with NAMD.[24] Docking experiments were conducted using Autodock 4.2[25] to derive the binding conformation of G6P and CHLs in the modeled T1. A grid was set on the modeled T1 with grid spacing dimensions of $X = 58$ Å, $Y = 54$ Å, and $Z = 52$ Å, centered on T1, and 100 GALS runs were executed with a population size of 500 and an electrostatic potential value of 0.1660. This value of 0.1660 was predicted using the software Adaptive Poisson—Boltzmann Solver.[26] Quantum mechanics (QM) optimization of the structures was done using GAMESS.[27] To assess the binding affinity of G6P and CHLs with modeled T1, binding free energies were calculated using the empirical scoring function provided by Autodock 4.2.[28]

$$G_{binding} = G_{vdw} + G_{elec} + G_{hbond} + G_{desolv} + G_{tors} \qquad (6)$$

where G_{vdW} is the Lennard-Jones potential (with 0.5 Å smoothing), G_{elec} is the Solmajer and Mehler distance-dependent dielectric, G_{hbond} is the H-bonding potential with Goodford directionality, G_{desolv} is the charge-dependent variant of Stouten pairwise atomic solvation parameters, and G_{tors} is the number of rotatable bonds. The intermolecular energy between the ligands and modeled T1 was extracted from the docking experiments and analyzed using MD simulations.[29]

5.3. Steered Molecular Dynamics of the T1–G6P Complex: Determination of the Pulling Velocity and Spring Constant. Considering the structure of T1 like that of a funnel with a wide mouth through which the G6P enters, SMD was carried out by having a harmonic spring attached to the center of mass of the G6P, moving with a steady velocity in *a* direction heading toward the neck and then to the stem of the funnel through which G6P is translocated. The transducer spring constant was $k = 1686$ kJ mol^{-1} nm^{-2} (units used by GROMACS package, 2.8 N/m), and this value is the physical stiffness of the linker and was taken from a range of applied velocities ($v = 0.15-15$ m/s). Umbrella sampling was conducted for 22 frames extracted from every 1.5 Å movement made across the channel. A sequence of windows covers the intermediary processes, and MD simulation is carried out in every window. The complex of modeled T1 and G6P was simulated four times for 5 nanoseconds (ns) using the GROMACS 2019.4 package[30,31] with the AMBER99SB force field. The charges for G6P were assigned using Antechamber [version 17.3 AM1BCC], and the topologies files for GROMACS were prepared using the program Topolbuild, developed by Bruce D. Ray (personal communication). AMBER 99SB and GAFF force fields [AMBER99SB-ILDN] were consistently used for defining charges and topologies for the modeled T1 and G6P, respectively. MD simulations were carried out under optimal temperature and pressure conditions. Simulations were conducted by placing modeled T1 in a box with dimensions of $6.640 \times 6.487 \times 5.643$ (nm) containing water molecules (SPC/E model). The total charge of the system having ~54,914 atoms was neutralized using K$^+$ ions. 50,000 steps of steepest descent minimization and 200 ps position restrained dynamics (PSD) were used to equilibrate the water molecules. T1 and the heavy atoms of the G6P were restrained, while water atoms were allowed to move in PSD. The electrostatics were calculated using the PME method with a real space cutoff of 10 Å, using an order of 4 and a relative tolerance between long- and short-range energies of $10-5$. Short-range interactions were evaluated using a neighbor list of 10 Å, and the Lennard-Jones (LJ) interactions and the real space electrostatic interactions were truncated at 9 Å. The temperature was maintained using V-rescale; hydrogen bonds were constrained using the LINCS algorithm.[32] The free energy change in every window was calculated using the sampled distribution of the system along the reaction coordinate.[33,34] Every conformation derived from the 5 ns × 4 simulation was used to perform 22 umbrella samplings.

5.4. Novel Scoring Function Designed to Rank the CHLs Docked with T1. The T1–G6P complex was used to make a weight matrix by using the atomic contacts between catalytically competent docked conformations of G6P with T1. The generated weights were used to score the docked formations of CHLs and rank them the same. The equations of the scoring function are explained in the Results section.

ASSOCIATED CONTENT

ⓢ Supporting Information

The Supporting Information is available free of charge at https://pubs.acs.org/doi/10.1021/acsomega.3c07267.

> Database of 43 chlorogenic acids from various plant sources, information on modeling T1, Ramachandran plot for the modeled T1 protein, and docking Scores of 43 CHLs calculated using the customized scoring method (PDF)

AUTHOR INFORMATION

Corresponding Author

Pravin Kumar Ramalingam − *Department of Computational Biology and AI, Kcat Enzymatic Pvt Ltd, Bangalore, Karnataka 560005, India;* ⓞ orcid.org/0000-0002-1466-0339; Email: pravin.k@kcat.co.in

Authors

Manikandan Chandrasekaran − *Department of Computational Biology and AI, Kcat Enzymatic Pvt Ltd, Bangalore, Karnataka 560005, India*

Poonam Gupta − *Department of Computational Biology and AI, Kcat Enzymatic Pvt Ltd, Bangalore, Karnataka 560005, India*

Vinod Nelamangala Umesh − *Department of Computational Biology and AI, Kcat Enzymatic Pvt Ltd, Bangalore, Karnataka 560005, India*

Tharun Bharadwaj − *Department of Computational Biology and AI, Kcat Enzymatic Pvt Ltd, Bangalore, Karnataka 560005, India*

Naveen Banchallihundi Krishna − *Department of Computational Biology and AI, Kcat Enzymatic Pvt Ltd, Bangalore, Karnataka 560005, India*

Roopa Lalitha − *Department of Computational Biology and AI, Kcat Enzymatic Pvt Ltd, Bangalore, Karnataka 560005, India*

Gladstone Sigamani Gunaseelan − *Department of Computational Biology and AI, Kcat Enzymatic Pvt Ltd, Bangalore, Karnataka 560005, India*

Complete contact information is available at:
https://pubs.acs.org/10.1021/acsomega.3c07267

Author Contributions

The manuscript was written through contributions of all authors. All authors have given approval to the final version of the manuscript.

Notes

The authors declare no competing financial interest.

ACKNOWLEDGMENTS

ABBREVIATIONS

CHLs, chlorogenic acids; SMD, steered molecular dynamics; T1, translocase-I; G6P, glucose-6-phosphatase; T1-G6P, T1 in complex with G6P

■ REFERENCES

(1) Greenberg, J. A.; Owen, D. R.; Geliebter, A. Decaffeinated Coffee and Glucose Metabolism in Young Men. *Diabetes Care* **2010**, *33* (2), 278−280.

(2) Reis, C. E. G.; Dórea, J. G.; da Costa, T. H. M. Effects of Coffee Consumption on Glucose Metabolism: A Systematic Review of Clinical Trials. *J. Tradit. Complementary Med.* **2019**, *9*, 184−191.

(3) Naismith, D. J.; Akinyanju, P. A.; Szanto, S.; Yudkin, J. The Effect in Volunteers of Coffee and Decaffeinated Coffee on Blood Glucose, Insulin, Plasma Lipids and Some Factors Involved in Blood Clotting. *Ann. Nutr. Metab.* **1970**, *12* (3), 144−151.

(4) Battram, D. S.; Arthur, R.; Weekes, A.; Graham, T. E. The Glucose Intolerance Induced by Caffeinated Coffee Ingestion Is Less Pronounced than That Due to Alkaloid Caffeine in Men. *J. Nutr.* **2006**, *136* (5), 1276−1280.

(5) Hemmerle, H.; Burger, H. J.; Below, P.; Schubert, G.; Rippel, R.; Schindler, P. W.; Paulus, E.; Herling, A. W. Chlorogenic Acid and Synthetic Chlorogenic Acid Derivatives: Novel Inhibitors of Hepatic Glucose-6-Phosphate Translocase. *J. Med. Chem.* **1997**, *40* (2), 137−145.

(6) Rojas-González, A.; Figueroa-Hernández, C. Y.; González-Rios, O.; Suárez-Quiroz, M. L.; González-Amaro, R. M.; Hernández-Estrada, Z. J.; Rayas-Duarte, P. Coffee Chlorogenic Acids Incorporation for Bioactivity Enhancement of Foods: A Review. *Molecules* **2022**, *27*, 3400.

(7) Charkoudian, L. K.; Farrell, B. P.; Khosla, C. Natural Product Inhibitors of Glucose-6-Phosphate Translocase. *MedChemComm* **2012**, *3*, 926.

(8) Parker, J. C. Glucose-6-Phosphate Translocase as a Target for the Design of Antidiabetic Agents. *Drugs Future* **2001**, *26* (7), 687−693.

(9) Belkaid, A.; Copland, I. B.; Massillon, D.; Annabi, B. Silencing of the Human Microsomal Glucose-6-Phosphate Translocase Induces Glioma Cell Death: Potential New Anticancer Target for Curcumin. *FEBS Lett.* **2006**, *580* (15), 3746−3752.

(10) Ihara, K.; Kuromaru, R.; Hara, T. Genomic Structure of the Human Glucose 6-Phosphate Translocase Gene and Novel Mutations in the Gene of a Japanese Patient with Glycogen Storage Disease Type Ib. *Hum. Genet.* **1998**, *103* (4), 493−496.

(11) Bräuer, S.; Almstetter, M.; Antuch, W.; Behnke, D.; Taube, R.; Furer, P.; Hess, S. Evolutionary Chemistry Approach toward Finding Novel Inhibitors of the Type 2 Diabetes Target Glucose-6-Phosphate Translocase. *J. Comb. Chem.* **2005**, *7* (2), 218−226.

(12) Lin, L. Z.; Harnly, J. M. Identification of Hydroxycinnamoyl-quinic Acids of Arnica Flowers and Burdock Roots Using a Standardized LC-DAD-ESI/MS Profiling Method. *J. Agric. Food Chem.* **2008**, *56* (21), 10105−10114.

(13) Clifford, M. N.; Johnston, K. L.; Knight, S.; Kuhnert, N. Hierarchical Scheme for LC-MSn Identification of Chlorogenic Acids. *J. Agric. Food Chem.* **2003**, *51* (10), 2900−2911.

(14) Johnston, K. L.; Clifford, M. N.; Morgan, L. M. Coffee Acutely Modifies Gastrointestinal Hormone Secretion and Glucose Tolerance in Humans: Glycemic Effects of Chlorogenic Acid and Caffeine. *Am. J. Clin. Nutr.* **2003**, *78* (4), 728−733.

(15) Arion, W. J.; Canfield, W. K.; Ramos, F. C.; Schindler, P. W.; Burger, H. J.; Hemmerle, H.; Schubert, G.; Below, P.; Herling, A. W. Chlorogenic Acid and Hydroxynitrobenzaldehyde: New Inhibitors of Hepatic Glucose 6-Phosphatase. *Arch. Biochem. Biophys.* **1997**, *339* (2), 315−322.

(16) Clifford, M. N. Chlorogenic Acids and Other Cinnamates − Nature, Occurrence and Dietary Burden. *J. Sci. Food Agric.* **1999**, *79*, 362−372.

(17) Farah, A.; Donangelo, C. M. Phenolic Compounds in Coffee. *Braz. J. Plant Physiol.* **2006**, *18*, 23−36.

(18) Pereira, A. d. S.; Pereira, A. F. d. M.; Trugo, L. C.; Neto, F. R. d. A. Distribution of Quinic Acid Derivatives and Other Phenolic Compounds in Brazilian Propolis. *Z. Naturforsch. C* **2003**, *58* (7−8), 590−593.

(19) Comino, C.; Lanteri, S.; Portis, E.; Acquadro, A.; Romani, A.; Hehn, A.; Larbat, R.; Bourgaud, F. Isolation and Functional Characterization of a CDNA Coding a Hydroxycinnamoyltransferase Involved in Phenylpropanoid Biosynthesis in Cynara Cardunculus L. *BMC Plant Biol.* **2007**, *7*, 14.

(20) Zapesochnaya, G. G.; Kurkin, V. A.; Kudryavtseva, T. V.; Karasartov, B. S.; Cholponbaev, K. S.; Tyukavkina, N. A.; Ruchkin, V. E. Dicaffeolyquinic Acids from Helichrysum Italicum and Achillea Cartilaginea. *Chem. Nat. Compd.* **1992**, *28* (1), 40−44.

(21) Harborne, J. B.; Corner, J. J. Plant Polyphenols. 4. Hydroxycinnamic Acid-Sugar Derivatives. *Biochem. J.* **1961**, *81*, 242−250.

(22) Konczak, I.; Okuno, S.; Yoshimoto, M.; Yamakawa, O. Caffeoylquinic Acids Generated in Vitro in a High-Anthocyanin-Accumulating Sweet Potato Cell Line. *J. Biomed. Biotechnol.* **2004**, *2004* (5), 287−292.

(23) Do, P. C.; Lee, E. H.; Le, L. Steered Molecular Dynamics Simulation in Rational Drug Design. *J. Chem. Inf. Model.* **2018**, *58* (8), 1473−1482.

(24) Strack, D.; Gross, W.; Wray, V.; Grotjahn, L. Enzymic Synthesis of Caffeoylglucaric Acid from Chlorogenic Acid and Glucaric Acid by a Protein Preparation from Tomato Cotyledons. *Plant Physiol.* **1987**, *83* (3), 475−478.

(25) Phillips, J. C.; Braun, R.; Wang, W.; Gumbart, J.; Tajkhorshid, E.; Villa, E.; Chipot, C.; Skeel, R. D.; Kalé, L.; Schulten, K. Scalable Molecular Dynamics with NAMD. *J. Comput. Chem.* **2005**, *26*, 1781−1802.

(26) Steffen, C.; Thomas, K.; Huniar, U.; Hellweg, A.; Rubner, O.; Schroer, A. AutoDock4 and AutoDockTools4: Automated Docking with Selective Receptor Flexibility. *J. Comput. Chem.* **2010**, *31* (16), 2967−2970.

(27) Jurrus, E.; Engel, D.; Star, K.; Monson, K.; Brandi, J.; Felberg, L. E.; Brookes, D. H.; Wilson, L.; Chen, J.; Liles, K.; Chun, M.; Li, P.; Gohara, D. W.; Dolinsky, T.; Konecny, R.; Koes, D. R.; Nielsen, J. E.; Head-Gordon, T.; Geng, W.; Krasny, R.; Wei, G. W.; Holst, M. J.; McCammon, J. A.; Baker, N. A. Improvements to the APBS Biomolecular Solvation Software Suite. *Protein Sci.* **2018**, *27* (1), 112−128.

(28) Alexeev, Y.; Mazanetz, M. P.; Ichihara, O.; Fedorov, D. G. GAMESS As a Free Quantum-Mechanical Platform for Drug Research. *Curr. Top. Med. Chem.* **2013**, *12* (18), 2013−2033.

(29) Abraham, M. J.; Murtola, T.; Schulz, R.; Páll, S.; Smith, J. C.; Hess, B.; Lindahl, E. Gromacs: High Performance Molecular Simulations through Multi-Level Parallelism from Laptops to Supercomputers. *SoftwareX* **2015**, *1−2*, 19−25.

(30) Grubmüller, H.; Heymann, B.; Tavan, P. Ligand Binding: Molecular Mechanics Calculation of the Streptavidin-Biotin Rupture Force. *Science* **1996**, *271* (5251), 997−999.

(31) Hess, B.; Kutzner, C.; Van Der Spoel, D.; Lindahl, E. GROMACS 4: Algorithms for Highly Efficient, Load-Balanced, and Scalable Molecular Simulation. *J. Chem. Theory Comput.* **2008**, *4* (3), 435−447.

(32) Van Der Spoel, D.; Lindahl, E.; Hess, B.; Groenhof, G.; Mark, A. E.; Berendsen, H. J. C. GROMACS: Fast, Flexible, and Free. *J. Comput. Chem.* **2005**, *26*, 1701−1718.

(33) Hess, B.; Bekker, H.; Berendsen, H. J. C.; Fraaije, J. G. E. M. LINCS: A Linear Constraint Solver for Molecular Simulations. *J. Comput. Chem.* **1997**, *18* (12), 1463−1472.

(34) Kästner, J. Umbrella Sampling. *Wiley Interdisc. Rev.: Comput. Mol. Sci.* **2011**, *1*, 932−942.